Earth Planet. Sci. Lett. 676 (2026) 119784

Contents lists available at ScienceDirect

Earth and Planetary Science Letters

journal homepage: www.elsevier.com/locate/epsl

Isotope effects (Cl, O, C) of heterogeneous electrochemistry induced by Martian dust activities

Neil C. Sturchio [a,*], Hao Yan [b,g,*], Alian Wang [c,*], W. Andrew Jackson [d], Huiming Bao [b,g], Chuck Y.C. Yan [c], Linnea J. Heraty [a], Yu Wei [b,g], Quincy H.K. Qu [c,e], Kevin S. Olsen [f]

[a] Department of Earth Sciences, University of Delaware, Newark, DE 19713, USA
[b] International Center for Isotope Effects Research, State Key Laboratory of Critical Earth Material Cycling and Mineral Deposits, Nanjing University, Nanjing, 210023, China
[c] Department of Earth, Environmental and Planetary Sciences and McDonnell Center for Space Sciences, Washington University in St. Louis, St. Louis, MO 63130, USA
[d] Department of Civil, Environmental, and Construction Engineering, Texas Tech University, Lubbock, TX 79409, USA
[e] School of Space Science and Physics, Institute of Space Sciences, Shandong University, Weihai, Shandong, 264209, China
[f] Department of Physics, University of Oxford, Oxford OX1 3PU, United Kingdom
[g] Frontiers Science Center for Critical Earth Material Cycling, School of Earth Sciences and Engineering, Nanjing University, Nanjing, 210023, China

ARTICLE INFO

Editor: Dr O Mousis

Keywords:
Mars surface-atmosphere interactions
Dust activity
Electrostatic discharge
Kinetic isotope effects
Heterogeneous electrochemistry

ABSTRACT

Some oxidized compounds in Martian soils may form through heterogeneous electrochemistry (HEC) stimulated by electrostatic discharge (ESD) during dust storms and dust devils. To test this hypothesis, we conducted medium-strength ESD experiments in a Mars simulation chamber and analyzed the Cl, O, and C isotopic compositions of the resulting chloride, (per)chlorate, and carbonate products. These ESD products exhibit substantial mass-dependent depletions in heavy isotopes relative to the reactants: ε^{37}Cl from -11.3 ‰ to +2.0 ‰, ε^{18}O from -34.5 ‰ to -12.9 ‰, and ε^{13}C around -11.4 ‰. These results, when compared with isotopic measurements from recent Mars missions (ESA's ExoMars Trace Gas Orbiter and the Sample Analysis at Mars (SAM) instrument package aboard NASA's Curiosity rover) and Martian meteorites, indicate that HEC induced by Martian dust activities can account for a substantial portion of the (per)chlorates and carbonates identified at the surface of Mars and the HCl in its atmosphere.

1. Introduction

The surface of Mars is a dynamic environment in which dust storms and dust devils occur frequently and cause frictional electrification of colliding dust particles mobilized by wind (Eden and Vonnegut, 1973; Mills, 1977; Melnik and Parrot, 1998). Size separation of suspended particles having opposite charges can lead to charge separation. An electrostatic discharge (ESD) would occur where a sufficiently large electrical potential is present. ESD associated with Martian dust activities can occur under small potential gradients on the order of 20–25 kV m^{-1} (Mills, 1977; Melnik and Parrot, 1998) because of the thin Martian atmosphere and are most likely to occur near the surface (Rahman et al., 2023). During ESD events, energetic electrons collide with atmospheric molecules, producing a range of reactive species including ions, radicals, electronically excited neutrals, and oxidized molecular products (Wu et al., 2018). ESD-induced heterogeneous electrochemistry (HEC) has strong oxidation potentials (Wu et al., 2018) and may account for both the presence of abundant oxidized compounds (e.g., (per)chlorates) and the near-absence of organic carbon compounds detected in Martian soils (Bak et al., 2022).

Laboratory simulations of Martian ESD conditions have shown that chloride and chlorate salts subjected to ESD in a CO_2-rich atmosphere yield a variety of reaction products, including volatile chlorine species, oxides, carbonates, and (per)chlorates retained in residual salt phases (Wang et al., 2023). The present study was performed on a set of representative reactant and product samples similar to the ESD experiments (Wang et al., 2023) to characterize isotopic compositions of chlorine, oxygen, and carbon products, and to compare these results with available isotopic data for the Martian atmosphere and surface (obtained during orbiter and lander missions) and Martian meteorites. The isotope effects were quantified from the differences in isotopic compositions of reactants (CO_2, KCl, $MgCl_2$, $KClO_3$) and products

* Corresponding authors.
E-mail addresses: sturchio@udel.edu (N.C. Sturchio), yanhao@nju.edu.cn (H. Yan), alianw@levee.wustl.edu (A. Wang).

https://doi.org/10.1016/j.epsl.2025.119784
Received 29 August 2025; Received in revised form 14 November 2025; Accepted 8 December 2025
Available online 18 December 2025

(including volatile Cl deposited on upper electrodes, $KClO_3$ product extracted from residual KCl reactant salt, $KClO_4$ product extracted from residual $KClO_3$ reactant salt, and $MgCO_3$ product extracted from residual $MgCl_2$ reactant salt). The results of these isotopic measurements offer new insights into the potential role of ESD-induced HEC in shaping the geochemical and isotopic landscape of the Martian surface-atmosphere system.

2. Methods

The apparatus and procedures used in this study for the electrostatic discharge (ESD) experiments, along with the initial reactants and detected volatile species and free radicals, are described in the Supplementary Materials. These experiments were similar to those described by Wang et al. (2023). Methods for isotopic analysis of the reactants and selected reaction products are described below.

2.1. Chlorate and perchlorate purification

Chlorate (ClO_3^-) was extracted from the ESD irradiated KCl salts at Texas Tech University following the method of Jackson et al. (2021). The KCl reacted salt was sequentially extracted (3X) using acetone. The acetone solution was evaporated to dryness and the residue dissolved in milli-Q water. Trace perchlorate was removed by passing through a small column (1 − 2 mL) of a ClO_4^- specific bi-functional anion-exchange resin (Purolite™ A530E). This solution was then further purified by first evaporating to ~ 1 − 2 mL and adding CsCl (300 μL, 1.2 g/mL). This solution was stored at 4 °C until crystals formed. The crystals were removed and gently washed with ethanol. The samples were redissolved in milli-Q water and reacted with 1 − 2 mL of 3 % hydrogen peroxide (H_2O_2).

Perchlorate (ClO_4^-) was purified from ESD irradiated $KClO_3$. Reacted salts were dissolved in milli-Q water. The aqueous solution was passed through a column containing ClO_4^- selective anion exchange resin (Purolite™ A530E) (Gu et al., 2011; Hatzinger et al., 2018). Resin containing extracted ClO_4^- was washed with approximately five bed volumes of 4 M hydrochloric acid (HCl) to remove impurities (residual K^+ and ClO_3^- as well as HCO_3^-). The ClO_4^- was then eluted from the column with a solution of 1 M ferric chloride ($FeCl_3$) in 4 M HCl. The $FeCl_3$–HCl eluent solution (containing the eluted ClO_4^-) was neutralized with NaOH (pH ~ 7–8) to precipitate iron (Fe) as $Fe(OH)_3$. After Fe $(OH)_3$ precipitate was removed by centrifugation, the supernatant solution was collected and evaporated in an oven (T = 60 °C) until the volume was ~10 ml. This solution was passed through a series of clean up cartridges (Dionex™ OnGuard™) to remove Cl^-, SO_4^{-2} and residual organic matter. The eluted volume was then evaporated to ~ 1 ml and a small volume of cesium chloride (CsCl) solution (300 μL, 1.2 g/mL) was added to the ClO_4^- solution. This solution was stored at 4 °C until $CsClO_4$ crystals formed. Finally, the crystals were rinsed with ethanol and redissolved in milli-Q water prior to shipping to the University of Delaware for isotopic analysis. Extensive tests of the procedures used for ClO_3 and ClO_4 isotopic analysis confirmed negligible Cl and O isotope exchange during processing of samples (Gu et al., 2011; Hatzinger et al., 2018; Jackson et al., 2021).

2.2. Cl and O isotopic analysis of chlorides, chlorates, and perchlorate

Isotopic analyses of Cl and O in chloride reactants and products, chlorate reactant, and perchlorate product from the ESD experiments were conducted at the Environmental Isotope Science Laboratory (EISLab) of the University of Delaware, using methods described by Böhlke et al. (2017). Also analyzed at EISLab were the C and O isotope ratios of the CO_2 gas used in the ESD experiments conducted on KCl and $KClO_3$ in 2021–2022.

Briefly, each chloride salt was dissolved in high-purity water, and chloride was re-precipitated as AgCl by addition of $AgNO_3$ to the salt solution. The AgCl was sealed in a pre-baked, evacuated borosilicate tube with excess CH_3I and heated at 300 °C for two hours to transform AgCl to CH_3Cl. The CH_3Cl was purified by gas chromatography and cryo-focused from a He carrier gas stream. The He was pumped away and the CH_3Cl was warmed to room temperature and expanded into the source of a Thermo Fisher Delta V Plus isotope-ratio mass spectrometer (IRMS). Measurements of the $^{37}Cl/^{35}Cl$ ratio were made in dual-inlet mode at m/z 50 and 52. Results were normalized to $KClO_4$ isotope reference materials USGS-37 and USGS-38 (Böhlke et al. (2017).

The $KClO_3$ reactant salt and the purified perchlorate product (from solution trap) produced by ESD irradiation of $KClO_3$ were first transformed to $CsClO_4$ salts that were then sealed in evacuated borosilicate tubes and decomposed by heating to 620 °C for 30 min to produce CsCl salt and O_2 gas. The O_2 gas was removed by tube-cracking into an evacuated stainless-steel loop and cooled in liquid nitrogen to remove H_2O and CO_2 impurities. The purified O_2 gas was expanded into the source of the isotope-ratio mass spectrometer for measurement in dual-inlet mode at m/z 32, 33, and 34. Oxygen isotope ratios ($^{18}O/^{16}O$ and $^{17}O/^{16}O$) were normalized to $KClO_4$ isotope reference materials USGS-37 and USGS-38 ((Böhlke et al. (2017)). The CsCl salt residue from the $CsClO_4$ decomposition was rinsed from the borosilicate tube using warm high-purity water, then treated as described above for Cl isotope ratio analysis.

The $KClO_3$ produced by ESD irradiation of KCl was partially purified, but the presence of substantial nitrate impurity precluded analysis by the conventional IRMS method described above because the O isotope ratio would have represented a mixture of oxygen from ClO_3 and NO_3. Therefore, the $KClO_3$ product was measured by using a Thermo Fisher Exploris 240 Orbitrap instrument. An aliquot of the impure ClO_3 solution was mixed with LC-MS grade methanol (in a ratio of 1:9) and injected into the electrospray ionization source of the Orbitrap instrument in dual-syringe mode (Hilkert et al., 2021). A secondary isotope reference material measured previously by IRMS (RSIL-8 $KClO_3$; Sturchio et al., 2006) was used for single-point normalization of Cl and O isotope ratios obtained from the ClO_3^- isotopolog signals measured at nominal masses of 83.45, 84.45, 85.45, 86.45, and 87.45 amu.

2.3. C and O isotopic analyses of CO_2 and carbonate

The $MgCO_3$ measurements were conducted at the International Center for Isotope Effects Research (ICIER), Nanjing University. To determine the isotope compositions of $MgCO_3$ in the ESD products, we used the conventional phosphoric acid method (McCrea, 1950) to digest the carbonate and then measured the isotope compositions of the CO_2 released. However, since chloride can react with phosphoric acid to generate HCl under vacuum conditions, and HCl is difficult to separate from CO_2, a pretreatment step was required to extract $MgCO_3$ from the residual $MgCl_2$ and other ESD products.

The extraction procedure was as follows. The ESD product powders were placed in a sealed tube, which was flushed with N_2 for 10 min to remove any residual air. About 15 ml CO_2-free water was added to the tube with a syringe. After shaking the tube for 3 min to dissolve most of the sample powder, it was centrifuged, and the supernatant was discarded. This water rinsing process was repeated five times to ensure the removal of most chloride ions. The pH of the supernatant was measured, and none of the samples had a pH below 7.5, indicating that carbonate dissolution during rinsing was minimal. The remaining residue was then dried under vacuum conditions at 50 °C for 48 h. Finally, the dried solid was digested with 105 % H_3PO_4 at 90 °C to generate CO_2.

To assess the influence of the extraction procedure on the isotope composition of $MgCO_3$, we conducted control experiments using a powdered mixture with $MgCO_3$, MgO, $MgCl_2$, and $Mg(ClO_4)_2$ in proportions similar to those in the ESD product powders (Wang et al., 2023). The control experiments followed the same procedure as the ESD samples. The isotope composition of $MgCO_3$ was measured before and after the extraction to evaluate any potential alterations. The $\delta^{13}C$, $\delta^{18}O$,

and $\Delta^{17}O$ values of $MgCO_3$ after the extraction procedure are +2.01 ± 0.45 ‰, +28.50 ± 1.40 ‰, and –0.17± 0.02 ‰ (n = 8), respectively, identical to those of the initial $MgCO_3$ salt within the analytical errors ($\delta^{13}C$ = +2.60 ± 0.06 ‰, $\delta^{18}O$ = +29.27 ± 0.24 ‰, and $\Delta^{17}O$ = –0.14 ± 0.01 ‰, n = 3). The consistency in the isotope compositions of $MgCO_3$ indicates that isotope fractionation induced by the extraction procedure is negligible.

The $\delta^{13}C$ and $\delta^{18}O$ values of CO_2 used in $MgCl_2$ irradiation experiments conducted after 2022 were measured on a MAT 253 Plus mass spectrometer (Thermal Fisher scientific) in dual-inlet mode. Each analysis comprised five sample-standard bracketing cycles, achieving an external precision (1SD) of ± 0.02 ‰ for both isotopes. To measure $\Delta^{17}O$, we applied the Pt-catalyzed CO_2–O_2 oxygen isotope exchange technique for which details of the apparatus and procedure were described by Wei et al. (2024). Briefly, following $\delta^{18}O$ analysis, the residual CO_2 was retrieved from the IRMS bellow and reacted with a $\Delta^{17}O$-known O_2 at 750 °C for one hour in the presence of a Pt catalyst. The CO_2 and O_2 were then separated for subsequent analysis. The initial $\Delta^{17}O$ value of CO_2 was determined through mass balance calculations incorporating pre-calibrated isotope fractionation factors between CO_2 and O_2 at steady state. Long-term precision for $\Delta^{17}O$, based on repeated analyses of our working standards, was ± 0.008 ‰ (1SD, n = 50).

2.4. Isotope ratio notation

Values of isotope ratios are reported in δ notation in units of per mil (‰) relative to those of Vienna Standard Mean Ocean Water (VSMOW) for oxygen, Vienna PeeDee Belemnite (VPDB) for carbon, and Standard Mean Ocean Water (SMOC) for chlorine, after multiplication by 1000, as follows:

$$\text{Chlorine isotopes: } \delta^{37}Cl_{sample}\ (‰) = [(^{37}Cl/^{35}Cl)_{sample}/(^{37}Cl/^{35}Cl)_{SMOC}) - 1] \times 10^3 \quad (1)$$

$$\text{Carbon isotopes: } \delta^{13}C_{sample}\ (‰) = [(^{13}C/^{12}C)_{sample}/(^{13}C/^{12}C)_{VPDB}) - 1] \times 10^3 \quad (2)$$

$$\text{Oxygen isotopes: } \delta^{i}O_{sample}\ (‰) = [(^{i}O/^{16}O)_{sample}/(^{i}O/^{16}O)_{VSMOW}) - 1] \times 10^3 \quad (3)$$

where i denotes 17 or 18.

$\Delta^{17}O$, a measure of mass independence, is defined as:

$$\Delta^{17}O = ln(\delta^{17}O / 1000 + 1) - 0.528 ln(\delta^{18}O / 1000 + 1) \quad (4)$$

2.5. Isotope fractionation factors

Isotope fractionation factors are defined as $\alpha_{product\text{-}reactant}$=$R_{product}$/$R_{reactant}$, where R is the isotope ratio of the element of interest, e.g., $^{37}Cl/^{35}Cl$. Alternatively, the isotope fractionation can be expressed as an isotope enrichment factor, ε, in units of ‰, defined as ε = (α−1) × 1000. Isotope fractionations observed in this study are considered to be kinetic isotope effects.

3. Results

Detailed descriptions of the materials, apparatus, procedures, and analytical methods used for product characterization during electrostatic discharge experiments employed in this study are provided in Supplementary Materials, and are briefly summarized below.

3.1. Compositional environment

First, we need to understand the compositional environment created by ESD process in the simulation chamber that can affect the Cl, O, and C isotopic signatures. The chamber was filled with dry CO_2 (~3 ± 0.1 mbar) and has a 2-mm thick layer of powdered chloride (or chlorate) salt in an open SiO_2 cell facing the energetic electron beam. In situ plasma spectra (Fig. 1) were collected during the ESD process to detect volatile species and free radicals. Table 1 lists the assignments of the observed plasma lines.

Most plasma lines were from CO_2^+ and CO*, i.e., the breakdown products of CO_2 gas. Two strong plasma lines of O_I* (777 and 844 nm) appear in Fig. 1, corresponding to the transitions of O_I from ^5P to $^5S^0$ and from ^3P to $^3S^0$ (Table 1). The observations of the H_α line (~ 656 nm, representing a transition of $H_{n=3}$* → $H_{n=2}$*, E_K ~ 12.08 eV, Table 1) and a few N_2* lines (750 – 900 nm) in the plasma spectrum (Fig. 1) indicate minor residual air and H_2O vapor. Because the electron impact dissociation energy of H_2O (i.e., $e^- + H_2O \rightarrow H\cdot + OH\cdot + e^-$) is 5.11 eV (Lukes et al., 2008), the appearance of H_α line implies a portion of electrons in ESD has kinetic energy ≥ 17.19 eV.

During the ESD-driven HEC reactions, highly reactive radicals CO_2^+, CO*, O_I*, O_3, and minor H*, N_2* participate in the formation of oxychlorines and carbonates shown in Fig. 2 and affect their isotopic signatures.

3.2. ESD experiments and isotopic analysis

Initial reactants and post-ESD samples (including 72 post-ESD salt samples and two samples of volatile Cl deposited on the electrodes, Fig. 2) of 74 ESD experiments were characterized for their bulk chemical compositions, isotopic compositions of Cl, O, and C, and phase identifications. Among the 74 ESD experiments, there were 32 ESD-on-KCl, 22 ESD-on-$KClO_3$, and 20 ESD-on-$MgCl_2$ (Table S1). To obtain sufficient amounts of reaction products for isotopic analyses, sample from multiple experimental runs were combined. Apparent product yields were low because reactions occurred mainly on the reactant salt grains exposed at the surface of the salt powder, leaving residual unreacted material within grain interiors and in buried grains that were shielded by the overlying salt.

The quantifications of ESD-induced reaction products were obtained from the chemical analyses of the post-ESD salts (Wang et al., 2023). The isotopic compositions of reactants and selected reaction products extracted from the residual reactant salts were obtained in the current study. The volatile Cl_I* released during ESD experiments was collected in the form of dark colored deposits on the upper electrode, whose $\delta^{37}Cl$ was characterized in the current study. Other released volatile species (Fig. 2), including HClO, ClO_2, ClO_3, ClO_4, were collected and quantified using two solution traps (Wang et al., 2023). The isotopic compositions of volatile species collected in the solution traps were not analyzed in the current study.

3.3. Isotopic results for Cl-bearing reactants and products

The $\delta^{37}Cl$, $\delta^{18}O$, and $\delta^{17}O$ values of reactant CO_2, KCl, $MgCl_2$, and $KClO_3$, along with those of products $KClO_3$ and $KClO_4$ extracted from residual reactant salts, are presented in Table 2. The $\delta^{37}Cl$ values of the reactant salts ranged from −0.5 ‰ to +0.31 ‰, and the $\delta^{18}O$ value of the reactant CO_2 was −7.8 ‰. The $\delta^{37}Cl$ values of the residual KCl and $MgCl_2$ salts were not significantly different than their initial values, which is consistent with the fact that only small fractions of these reactants were converted to products (Fig. 2) (Wang et al., 2023). Two samples of chloride (mainly CuCl) deposited from volatile Cl_I onto the upper electrodes of the experimental chamber during two ESD experiments on $MgCl_2$ yielded $\delta^{37}Cl$ values of −9.72 ‰ and −11.1 ‰. The differences in $\delta^{37}Cl$ values between these CuCl deposits and the initial $MgCl_2$ reactant salt indicate diagnostic Cl isotope fractionation factors of 0.9887 and 0.9901 (or, $\varepsilon^{37}Cl_{ClI-MgCl2}$ values of −9.9 ‰ and −11.3 ‰, respectively). During ESD irradiation of $MgCl_2$ in another set of ESD experiments reported by Wang et al. (2020), in situ plasma emission spectra showed the first excited state of Cl atom (i.e., Cl_I*) in the vapor phase (Fig. 2), while post-experiment X-ray diffraction measurements on the solid film coating the upper electrode showed CuCl to be the major

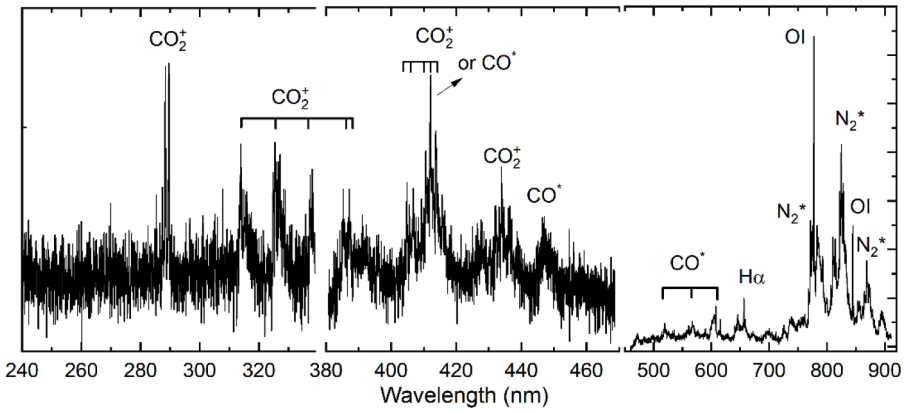

Fig. 1. Plasma spectra collected in situ during ESD in the simulation chamber filled with dry CO_2. Note the wavelength scale for 500–900 nm is different from those of 240–330 nm and 380–470 nm, for the purpose of showing the weak plasma lines in short wavelength ranges. The units on the Y-axis are counts per second. They are omitted here, because they were different for three spectral ranges shown in this figure, i.e., the ESD simulated plasma emission lines in CO_2 are much stronger in IR than in UV and VIS.

Table 1
Assignments of the plasma lines in Fig. 1 (Note: energy unit conversion 1 cm^{-1} = 0.00012398 eV).

Species	Observed (nm)	Relative Intensity (NIST)	Upper level (E_k)				Lower level (E_i)			Ref
			configuration	Term	cm^{-1}	eV	configuration	Term	cm^{-1}	
O_I*	777.5	**870**	$2s^22p^3(4S^\circ)$	^5P	86,631.5	***10.74***	$2s^22p^3(4S^\circ)$	$^5S^0$	73,768.2	NIST Atomic spectral line database (Kramida et al., 2024)
	844.7	**1000**	$3p$	^3P	86,631.1	***10.74***	$3s$	$^3S^0$	76,795.0	
	(630.0)	**0.005**	$2s^22p^4$	^1D	15,867.9	**1.97**	$2s^22p^4$	^3P	0	
	(715.7)	**210**	$2s^22p^3(^2D^0)$ $3p$	^1D	116,631.1	**14.46**	$2s^22p^3(^2D^0)$ $3s$	$^1D^0$	102,662.0	
	(788.6)	**80**	$2s^22p^3(^2p^0)3p$	^1D	128,594.9	**15.94**	$2s^22p^3(^2p^0)3s$	$^1p^0$	115,918.1	
CO*	412.5 519.4 560.5 607.6		$B^1\sum$				$A^1\Pi$			(Pearse and Gaydon, 1976)
	447.1 567.8		$d^3\Delta$				$a^3\Pi$			(Pearse and Gaydon, 1976; Endoh et al., 1982)
CO_2^+	288.3; 289.5		$B\sum_u^+$				$X^2\prod_g$			
	312.0~317.0 336.0~340.0 384.0~390.0 404.0~415.0 433.0~440.0		$A^2\Pi_u$				$X^2\prod_g$			(Pearse and Gaydon, 1976; Endoh et al., 1982)
Hα	656.3	***500,000***	*3*		*97,492.3*	***12.08***	*2*		82,258.9	NIST Atomic spectral line database (Kramida et al., 2024)
N_2*	771.6 773.8 775.1 782.9 799.4 825.1 828.1 869.1;		$B^3\prod_g$				$A^3\sum_u^+$			(Loftus and Krupenie, 1977)

Cl-bearing phase along with minor amounts of $Cu_2(OH)_3Cl$ and Cu_2OCl_2.

ESD irradiation of KCl produced a small amount of $KClO_3$, for which the $\delta^{37}Cl$ value was not significantly different than that of the initial KCl reactant (within the ±1.0 ‰ error of the Orbitrap measurement). However, the $\delta^{18}O$ value of the $KClO_3$ product was −42.1 ‰, which is a much more negative value than that of the CO_2 atmosphere in the experimental chamber. This −34.2 ‰ difference indicates $\alpha^{18}O_{KClO3-CO2} = 0.9655$ (or, $\varepsilon^{18}O_{KClO3-CO2} = -34.5$ ‰).

ESD irradiation of $KClO_3$ produced a small amount of $KClO_4$ (Fig. 2), for which the $\delta^{37}Cl$ value was +2.34 ‰. The difference between the $\delta^{37}Cl$ values of the $KClO_4$ product and the $KClO_3$ reactant indicated $\alpha^{37}Cl_{KClO4-KClO3} = 1.0020$ (or, $\varepsilon^{37}Cl_{KClO4-KClO3} = +2.0$ ‰). The −12.8 ‰ difference in $\delta^{18}O$ values between the $KClO_4$ product ($\delta^{18}O = -20.6$ ‰) and the $KClO_3$ reactant ($\delta^{18}O = -7.8$ ‰) indicated an apparent value of $\alpha^{18}O_{KClO4-KClO3} = 0.9871$ (or, $\varepsilon^{18}O_{KClO4-KClO3} = -12.9$ ‰).

3.4. Isotopic results for CO_2 reactant and $MgCO_3$ product

The $\delta^{13}C$, $\delta^{18}O$, and $\Delta^{17}O$ values of the initial CO_2 reactant and $MgCO_3$ product samples from ESD-$MgCl_2$ analyzed in this study, along with those for a reference $MgCO_3$ used for development of a method for the extraction of trace amounts of $MgCO_3$ from $MgCl_2$, are presented in Table 3. The consistency in the isotope compositions of the reference $MgCO_3$ before and after the extraction process confirms the robustness of our protocol for extracting $MgCO_3$ from a chloride-dominant mixture for isotope analysis (as described in Section 2.3).

The $\delta^{13}C$ and $\delta^{18}O$ values of $MgCO_3$ in the ESD product were −21.2 ‰ and +9.4 ‰, respectively, both significantly lower than those of the reactant CO_2 used in the ESD experiments (Table 3). As all C atoms in the $MgCO_3$ product are from the CO_2 reactant, the diagnostic carbon isotope fractionation between $MgCO_3$ and CO_2 associated with ESD processes

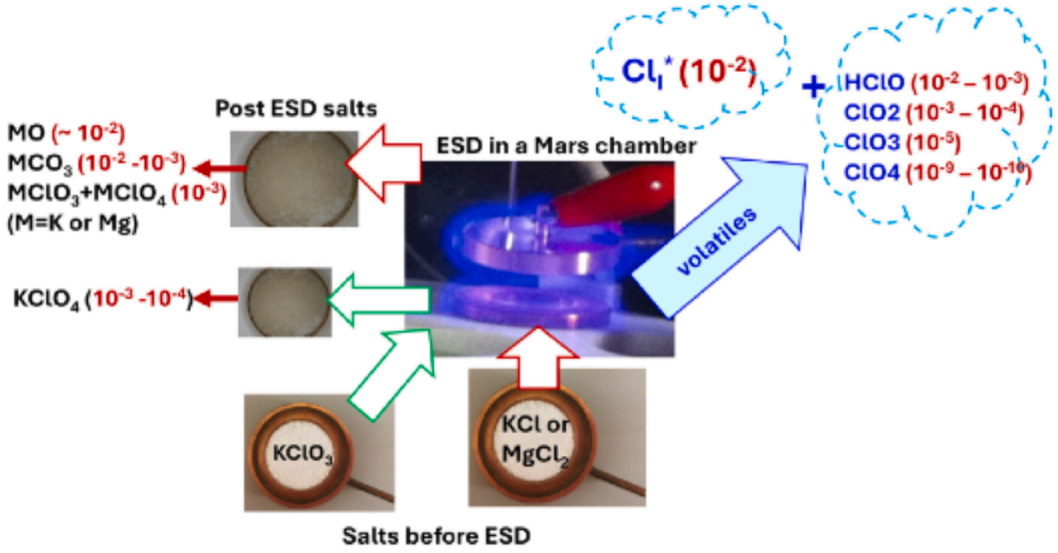

Fig. 2. Schematic diagram of ESD experimental procedure and the Cl distribution among the ESD products (expressed as the % of Cl from the reactant salts, based on results of Wang et al., 2023). Red arrows connect chloride salt reactants with most abundant solid products. Green arrows connect chlorate salt reactant with most abundant solid product. Blue arrow connects chloride salt reactants with two groups of Cl-bearing volatile products: Cl_I* that was deposited on the upper electrode as CuCl, and other ClO_X species that were retained by two solution traps. Cl_I* is a volatile chlorine atom in the 1st excited state.

should be equal to their $\delta^{13}C$ difference, i.e., $\varepsilon^{13}C_{MgCO3—CO2} = -11.4$ ‰. Similarly, all oxygen atoms in $MgCO_3$ are from CO_2 and its products in the ESD process, the diagnostic isotope fractionation between $MgCO_3$ and CO_2 ($\varepsilon^{18}O_{MgCO3—CO2}$) is estimated to be −22.8 ‰.

4. Discussion

4.1. Plasma spectra

The plasma spectra (Fig. 1) revealed that the major free radicals from CO_2 are CO_2^+, CO*, and O_I* (oxygen at 1st excited state, * = free radical). Among them, CO_2^+ is a product of electron impact ionization (EII) of CO_2 (Jackson et al., 2010):

$$e^- + CO_2 = 2e^- + CO_2^+ \quad (5)$$

Reaction (5) generates two more electrons, which would stimulate an electron avalanche, i.e., the subsequent chain reactions. The observation of CO_2^+ lines implied that the initial electrons in our ESD process have a minimum kinetic energy of ≥14 eV (Jackson et al., 2010). It also means other CO_2 breakdown processes that require less energy can occur, such as the electron-induced CO_2 dissociation reaction (ED of CO_2, requires 4.4 eV(Jackson et al., 2010), shown as several lines of CO* in Fig. 1.

$$e^- + CO_2 = CO^* + O^- \quad (6)$$

To reach the upper energy level (E_k) of the transitions of O_I from ^5P to $^5S^0$ and from ^3P to $^3S^0$ (Table 1, the 777 and 844 nm lines in Fig. 1), the required kinetic energy of the electron is 10.74 eV (Table 1), i.e., < 14 eV. In addition, for a transition from ^1D to ^3P, the required energy is 1.97 eV only (Table 1), which can occur in this ESD process. Table 1 shows that its emission line (~ 630 nm) has a relative intensity 10^{-6} times weaker than the 844 nm line, hard to detect. Another two transitions of oxygen that involve the ^1D spectral term cannot be excluded since their required energies are 14.46 and 15.94 eV (< 17.19 eV required by the H_α line). Overall, the detected O_I* radicals in our ESD experiments have the spectral terms of ^1D, ^3P, and ^5P

In an early set of similar experiments (Wu et al., 2018), O_3 was detected using IR and UV spectroscopy in the exhaust gases (Figure S3). Normally, O_3 would form through a 3-step reaction (Hokazono et al., 1991; Skalny et al., 2007):

$$e^- + CO_2 \rightarrow CO + O + e^- \quad (7)$$

$$O + O + CO_2 \rightarrow O_2 + CO_2 \quad (8)$$

$$O + O_2 + CO_2 \rightarrow O_3 + CO_2 \quad (9)$$

However, the quantity of O_3 may be much less than that of O_I* from the direct breakdown of CO_2.

4.2. Comparison of ESD-driven Cl and O isotope fractionation results with those of ozone- and UV-driven oxidation reactions in aqueous media

The isotopic compositions of Cl and O in chlorate and perchlorate produced experimentally under ozone- and UV-driven oxidation conditions were examined recently (Estrada et al., 2021). The experiments of Estrada et al. (2021) were done to elucidate the natural origins of terrestrial perchlorate and chlorate. Most of the experiments reported by Estrada et al. (2021) were performed in aqueous media, with initial reactants including solutions of the salts NaCl, $Ca(OCl)_s$, $NaClO_2$, and ClO_2 gas, as well as one dry ozone oxidation experiment with NaCl.

4.2.1. Chlorine isotope comparisons

All aqueous ozone-driven oxidation experiments involving any of the reactants listed above produced perchlorate and chlorate having substantial ^{37}Cl enrichments, with $\delta^{37}Cl$ values from +6 ‰ to +15 ‰ relative to those of the reactants (Estrada et al., 2021). Only in the dry ozone oxidation experiment involving NaCl did the perchlorate product have a more negative $\delta^{37}Cl$ value (by −3.5 ‰) than the reactant. All aqueous UV-driven oxidation experiments also produced perchlorate and chlorate having substantial ^{37}Cl enrichments, with $\delta^{37}Cl$ values from +5 ‰ to +19 ‰ relative to those of the reactants. The results of the present study show that ESD-driven oxidation of Cl produces (per) chlorates having smaller ^{37}Cl enrichments than those observed in aqueous ozone- and UV-driven oxidation experiments, with ESD-produced $KClO_4$ having a $\delta^{37}Cl$ value about +2 ‰ more positive than the reactant $KClO_3$, and ESD-produced $KClO_3$ having a $\delta^{37}Cl$ value within error of the reactant KCl.

4.2.2. Oxygen isotope comparisons

Comparison of the results of the oxygen isotope effects between the

Table 2
Chlorine and oxygen isotope compositions of experimental reactants and products of KCl and $KClO_3$ irradiations.

Sample name	$\delta^{37}Cl$ (SMOC, ‰)	1σ	$\delta^{18}O$ (VSMOW, ‰)	1σ	$\Delta^{17}O$ (VSMOW, ‰)	1σ	n[a]
Reactants							
KCl	−0.5	0.2	—	—	—	—	2
$MgCl_2$	+0.2	0.3	—	—	—	—	2
$KClO_3$	+0.3	0.1	−7.8	0.5	+0.5	0.2	2
CO_2[b]	—	—	−7.9	0.4	—	—	4
Products							
#708-Cl_I deposit on electrode (7-h ESD-on-$MgCl_2$)	−9.7	0.1	—	—	—	—	2
#709-Cl_I deposit on electrode (7-*h* ESD-on-$MgCl_2$)	−11.1	0.1	—	—	—	—	1
Extracted $KClO_3$ (15 samples; 7-h ESD-on-KCl) [†]	−0.1	1.0	−42.1	2.3	−0.9	3.4	2
Extracted $KClO_4$ (22 samples; 7-h ESD-on-$KClO_3$)	+2.3	0.2	−20.6	0.4	−0.9	0.2	2
7-h ESD-on-KCl (3 residual KCl samples combined)	−0.3	0.3	—	—	—	—	6
7-h ESD-on-$MgCl_2$ (one residual $MgCl_2$ sample)	0.0	0.1	—	—	—	—	1

[a] n = number of replicate analyses.
[b] CO_2 used in 2021–2022 for KCl and $KClO_3$ irradiation experiments; $\Delta^{17}O$ not measured.
[†] measurement by Orbitrap-MS with single-point normalization to USGS-RSIL-8 $KClO_3$ ($\delta^{37}Cl = +0.53$ ‰; $\delta^{18}O = -25.3$ ‰; $\Delta^{17}O = 0.0$ ‰).

Table 3
Carbon and triple oxygen isotope compositions of $MgCl_2$-ESD products.

Sample name	$\delta^{13}C$ (VPDB, ‰)	1σ	$\delta^{18}O$ (VSMOW, ‰)	1σ	$\Delta^{17}O$ (VSMOW, ‰)	1σ	n
Initial CO_2	−9.9	0.1	+32.9	0.2	−0.14	0.02	4
$MgCl_2$ *	−21.22	-	+9.35	-	−0.10	-	1

* Mixture of $MgCO_3$, MgO, $MgCl_2$, $Mg(ClO_4)_2$, and $Mg(ClO_3)_2$. Carbonate was extracted for isotopic analysis from combined residues from 17 separate 7-hour ESD experiments on $MgCl_2$.

ESD experiments of the present study and the ozone and UV experiments of Estrada et al. (Estrada et al., 2021) is complicated by the fact that the present study involved ESD-driven reactions on chloride or chlorate salts in a low-pressure CO_2 atmosphere whereas the ozone- and UV-driven experiments involved reactions involved mostly different reactants (chloride, hypochlorite, and chlorite salts, and ClO_2 gas) took place in a liquid aqueous medium at ~1 atm pressure. Nonetheless, one major difference between ozone-driven reactions and both ESD- and UV-driven reactions is that the perchlorates produced with ozone, regardless of Cl-bearing reactant, tend to have significant mass-independent oxygen isotope fractionation with $\Delta^{17}O$ values ranging from +12.0 ‰ to +32.9 ‰ (Estrada et al., 2021). Chlorate produced during ozone oxidation reactions also shows mass-independent oxygen isotope fractionation but to a lesser extent, with $\Delta^{17}O$ values from 0.0 ‰ to +7.7 ‰ (Estrada et al., 2021). In UV-driven reactions, $\Delta^{17}O$ values of chlorate and perchlorate are all within the range from −2.1 ‰ to +1.0 ‰ (Estrada et al., 2021). In contrast, no significant mass-independent oxygen isotope fractionation is evident in the ESD-driven reaction products (chlorate, perchlorate, and carbonate), as evidenced by the invariant $\Delta^{17}O$ values between reactants and products.

There are multiple possible sources of oxygen in the $KClO_4$ product from ESD experiments: fixed oxygen atoms in reactant $KClO_3$, reactive oxygen species produced from ESD-breakdown of CO_2, and reactive oxychlorine radical species produced from ESD-breakdown of $KClO_3$. Therefore, the difference in $\delta^{18}O$ values between $KClO_4$ and $KClO_3$ is difficult to interpret in terms of a specific reaction pathway in these experiments. However, the oxygen atoms in oxychlorine species on Mars would likely be derived from ESD-breakdown of CO_2. All ESD-driven reactions producing more-oxidized products from Cl-bearing substrates in the present study have large negative $\varepsilon^{18}O$ values. This pattern is typical of kinetic isotope effects that accompany rapid, irreversible reactions.

4.3. Comparison of ESD-driven C and O isotopic fractionations in carbonates with those in carbonates from aqueous solution

Most carbonate minerals on Earth and, potentially, on Mars form under aqueous conditions. The $\delta^{13}C$ and $\delta^{18}O$ signatures of aqueous carbonates have been extensively studied, as they are intimately linked to the carbon and water cycles. In such systems, the isotopic compositions of carbonate minerals are controlled primarily by those of dissolved inorganic carbon (DIC) species in solution, which can in turn be modified by isotopic exchange with ambient CO_2 and water.

4.3.1. Carbon isotope comparisons

Under equilibrium conditions, carbonate minerals typically exhibit $\delta^{13}C$ values that are 0–2 ‰ higher than those of the corresponding DIC and approximately 8–10 ‰ higher than that of ambient CO_2 at temperatures between 0 and 20 °C (Mook et al., 1974; Romanek et al., 1992). This enrichment supports the role of carbonate precipitation as a sink for $^{13}CO_2$ in planetary atmospheres, including Mars. However, under non-equilibrium conditions, carbonate minerals can become either enriched or depleted in ^{13}C relative to the ambient CO_2, depending on the specific pathways and environmental settings of their formation.

At near-neutral to mildly alkaline pH, carbonate precipitation is commonly driven by processes such as bicarbonate (HCO_3^-) dehydration and CO_2 degassing, which can induce substantial kinetic carbon isotope fractionation (Marlier and O'Leary, 1984). During bicarbonate dehydration, the kinetic isotope fractionation between HCO_3^- and CO_2 can be as large as 10–30 ‰ (depending on dehydration rates) (Yan et al., 2020), leading to progressive ^{13}C enrichment of the residual DIC pool via Rayleigh distillation. Carbonates precipitating from such enriched DIC reservoirs can inherit high $\delta^{13}C$ values. Cryogenic carbonate is an example, with $\delta^{13}C$ values as much as +25 ‰ relative to ambient CO_2 (Clark and Lauriol, 1992). In contrast, under hyperalkaline conditions, such as those produced during serpentinization of ultramafic rocks, CO_2 hydroxylation becomes the dominant process driving carbonate precipitation. This pathway is associated with substantial ^{13}C depletion (up to −18 ‰ relative to ambient CO_2), owing to kinetic fractionation during the hydroxylation reaction. Both types of carbonate formation described above have been proposed to occur on Mars (Burtt et al., 2024; Ehlmann et al., 2010).

The $\delta^{13}C$ values of carbonates produced in our ESD experiments fall within the range observed for carbonates precipitated from hyperalkaline solutions, indicating strong ^{13}C depletion relative to the CO_2

reactant. This suggests that ESD-induced heterogeneous electrochemical reactions associated with Martian dust activity could generate carbonates with $\delta^{13}C$ signatures similar to those formed under hyperalkaline aqueous conditions. However, some ESD-produced carbonates are amorphous, offering a potential textural or mineralogical criterion to distinguish them from the more-crystalline carbonates formed in aqueous environments.

4.3.2. Oxygen isotope comparisons

Oxygen isotope exchange between DIC and water proceeds rapidly at near-neutral to mildly alkaline pH (Beck et al., 2005), meaning that the $\delta^{18}O$ values of aqueous carbonates generally reflect the isotopic composition of the parent water. At equilibrium, carbonate minerals are enriched in ^{18}O by approximately 25–35 ‰ relative to water at 0–20 °C (Chacko et al., 2001). Although CO_2 is more enriched in ^{18}O than carbonate minerals by ~10 ‰ under equilibrium conditions, its influence is typically negligible in aqueous settings due to the rapid oxygen exchange with water.

An exception occurs in hyperalkaline environments, where oxygen isotope exchange between DIC and water is suppressed. In these settings, carbonate minerals can preserve the $\delta^{18}O$ signature of their source components, such that typically 2/3 of the oxygen atoms derive from CO_2 and 1/3 from hydroxide (OH^-) in solution (Clark et al., 1992). Assuming both CO_2 and OH^- are in equilibrium with water, the resulting carbonate would have $\delta^{18}O$ values approximately 26 ‰ lower than those of ambient CO_2. The magnitude of the oxygen isotope fractionation between CO_2 and OH^- in equilibrium with water under hyperalkaline conditions is apparently comparable to that between CO_2 and atomic oxygen produced during ESD, despite distinct formation mechanisms. The ESD-induced carbonate formation pathway, although fundamentally non-aqueous and electrochemical, produces oxygen isotope signatures coincidentally similar to those of carbonates formed under hyperalkaline aqueous conditions.

The $\Delta^{17}O$ values of the reactant CO_2 and the $MgCO_3$ in the ESD products are analytically indistinguishable, indicating that oxygen isotope fractionation between O atoms added to solid products and CO_2 is mass-dependent. The relatively large oxygen isotope fractionation as well as the mass-dependent-fractionation behavior is consistent with the results of CO electron-discharge experiments (Wei et al., 2024). Although O_3 is detected as a product in the ESD experiments (Figure S3) (Wu et al., 2018), the mass-dependent isotope fractionation between $MgCO_3$ and CO_2 indicates that the quantity of ESD-generated O_3 is insufficient to affect the $\Delta^{17}O$ values of carbonate reaction products (cf. Shaheen et al., 2010)

4.4. Comparison of in-situ and meteorite data from Mars with the ESD experimental results

To evaluate the hypothesis that ESD-driven heterogeneous electrochemistry reactions could account for the presence of oxidized compounds detected at the surface of Mars, we compare the experimental isotope effects measured in the present study with isotopic data from recent Mars missions and Martian meteorite studies. In-situ isotopic measurements of Mars' atmosphere and surface materials that are pertinent to the present experimental study are mainly limited to those obtained by two recent missions. Atmospheric data include chlorine isotope ratios of atmospheric HCl measured by the mid-infrared spectrometer aboard the European Space Agency's ExoMars Trace Gas Orbiter (Trokhimovskiy et al., 2021; Liuzzi et al., 2021) and carbon and oxygen isotope ratios of atmospheric CO_2 measured by the near-infrared tunable diode laser spectrometer (TLS) of the Sample Analysis at Mars (SAM) instrument package aboard NASA's Curiosity rover, which landed on Mars in August 2012 (Webster et al., 2013). Chlorine isotope ratios of Cl released as HCl were measured by the SAM quadrupole mass spectrometer by heating sedimentary rocks and sand in Gale Crater and measuring the $H^{37}Cl/H^{35}Cl$ ratio in evolved gas, which was presumably derived from thermal decomposition of (per)chlorate and/or chloride minerals (Glavin et al., 2013; Farley et al., 2016). Also measured by SAM during evolved gas measurements in Gale Crater was the isotopic composition of CO_2 released by heating drilled sedimentary rock and Rocknest aeolian drift material (Burtt et al., 2024; Leshin et al., 2013; Franz et al., 2020).

In addition to the in-situ isotopic data from Mars, there are numerous data available from studies of meteorites of Martian origin. The meteorite data include chlorine isotope ratios measured in bulk rocks, mineral separates, and water-soluble leachates (Williams et al., 2016; Bellucci et al., 2017) and carbon and oxygen isotope ratios measured in bulk rocks and carbonate minerals (Grady et al., 2004; Romanek et al., 1994; Jull et al., 1995; Valley et al., 1997, 1997; Niles et al., 2005; Shaheen et al., 2015).

4.4.1. Chlorine isotopes in chlorides and (per)chlorates

The chlorine isotope data from in-situ measurements and meteorite studies are compared with experimental results from the present study in Fig. 3. No in situ oxygen isotope data are yet available for Martian (per)chlorates. Igneous rocks (meteorites) from Mars have $\delta^{37}Cl$ values in the range of −3.8 ‰ to +1.8 ‰, with one anomalous value of +8.6 ‰ measured in a regolith breccia sample (Williams et al., 2016). According to Sharp et al. (2016), meteorites representative of the Martian mantle have $\delta^{37}Cl$ values in the range of −4 ‰ to −3 ‰, and meteorites representative of the Martian crust have $\delta^{37}Cl$ values in the range of 0 ‰ to +2 ‰.

Volatile Cl_I* atoms released to the atmosphere by ESD processes acting on Martian surface materials would become depleted in ^{37}Cl by ~10 ‰ to 11 ‰ relative to the source material, according to our experimental results. This would produce atmospheric HCl having negative $\delta^{37}Cl$ values, consistent with in-situ measurements (Liuzzi et al., 2021; Trokhimovskiy et al., 2021). The ^{37}Cl-depleted atmospheric HCl produced by ESD processes would react with silicate and oxide minerals on the surface, resulting in secondary chloride salts having negative $\delta^{37}Cl$ values. The high yield of volatile Cl_I* produced from chloride salts during the ESD process ($\sim 10^{-2}$ in 7h-ESD, Fig. 2), in concert with recycling of ^{37}Cl-depleted salts by dust activities (Fig. 5), could cause progressive ^{37}Cl-depletion toward the extreme negative $\delta^{37}Cl$ values (as low as −51 ‰) reported by Farley et al. (2016). Such progressive depletion in $\delta^{37}Cl$ values of surficial deposits would be most effective where the ^{37}Cl-depleted salts accumulate in thin layers at the surface and are subject to multiple ESD events (Fig. 5).

4.4.2. Carbon and oxygen isotopes in carbonates

The carbon and oxygen isotope data from in-situ measurements and meteorite studies are compared with experimental results from the present study in Fig. 4. The most precise available measurements of the C and O isotope compositions in atmospheric CO_2 at Martian surface were made with the Sample Analysis at Mars' Tunable Laser Spectrometer (SAM/TLS) on the Curiosity Rover, yielding $\delta^{13}C = +46 \pm 4$ ‰ and $\delta^{18}O = +48 \pm 5$ ‰ (shown as gray vertical bars in Fig. 3) (Webster et al., 2013). Carbon and oxygen isotope ratios of carbonate minerals in meteorites are widely varied, with $\delta^{13}C$ values ranging from −20 ‰ to +60 ‰ and $\delta^{18}O$ values ranging from −20 ‰ to +45 ‰ (Romanek et al., 1994; Jull et al., 1995; Valley et al., 1997, 1997; Niles et al., 2005; Shaheen et al., 2015; Carr et al., 1985; Farquhar and Thiemens, 2000). Martian mantle carbon has an estimated $\delta^{13}C$ value of -20 ± 4 ‰, based on stepped combustion and high-resolution mass spectrometry measurements of carbon released from the dunite meteorite Chassigny and 11 shergottites (Grady et al., 2004; Steele et al., 2012. Carbonate from aeolian samples on Mars measured by SAM (Leshin et al., 2013; Williams et al., 2016) has broad ranges of $\delta^{13}C$ and $\delta^{18}O$ values similar to those of the carbonate minerals measured in Mars meteorites. In contrast, carbonates from drilled sedimentary rocks measured by SAM within Gale Crater have a distinct range of $\delta^{13}C$ values from $+72 \pm 2$ ‰ to $+110 \pm 3$ ‰, attributed to a combination of kinetic isotope effects driven by

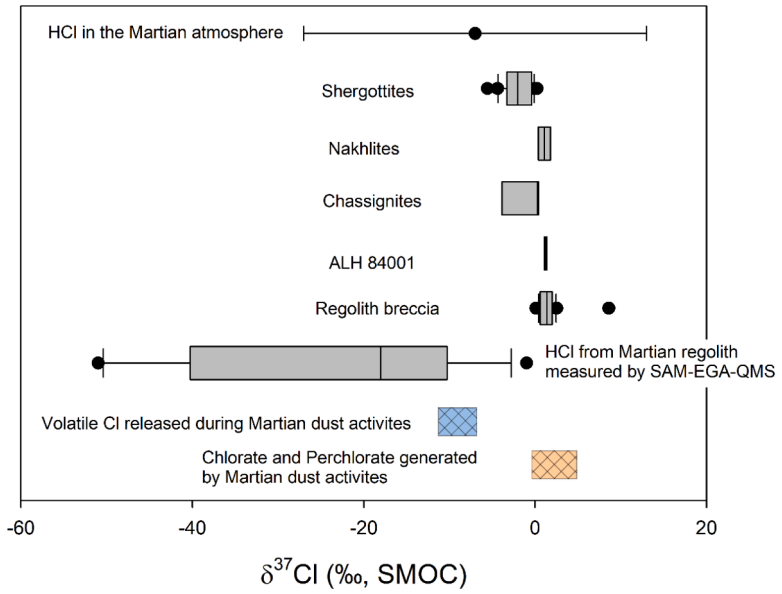

Fig. 3. Comparison of chlorine isotope compositions in chlorides and (per)chlorates from the ESD experiments with in-situ and meteorite data from Mars. The estimated isotope compositions of Cl species generated by Martian dust activities based on the isotope fractionation factor calibrated in this study. The blue and orange textured bars indicate the range of δ^{37}Cl values of volatile Cl and (per)chlorate generated by Martian dust activities assuming a range of δ^{37}Cl of the starting chloride identical to that of regolith breccia. The δ^{37}Cl values of different Cl reservoirs on Mars are also shown for comparison. These reservoirs include: HCl in the Martian atmosphere (Trokhimovskiy et al., 2021); shergottites, nakhlites, chassignites, ALH 84,001, and regolith breccia (Williams et al., 2016; Bellucci et al., 2017); and HCl released from oxychlorine compounds in the Martian regolith as measured in situ by the SAM-EGA-QMS (Farley et al., 2016).

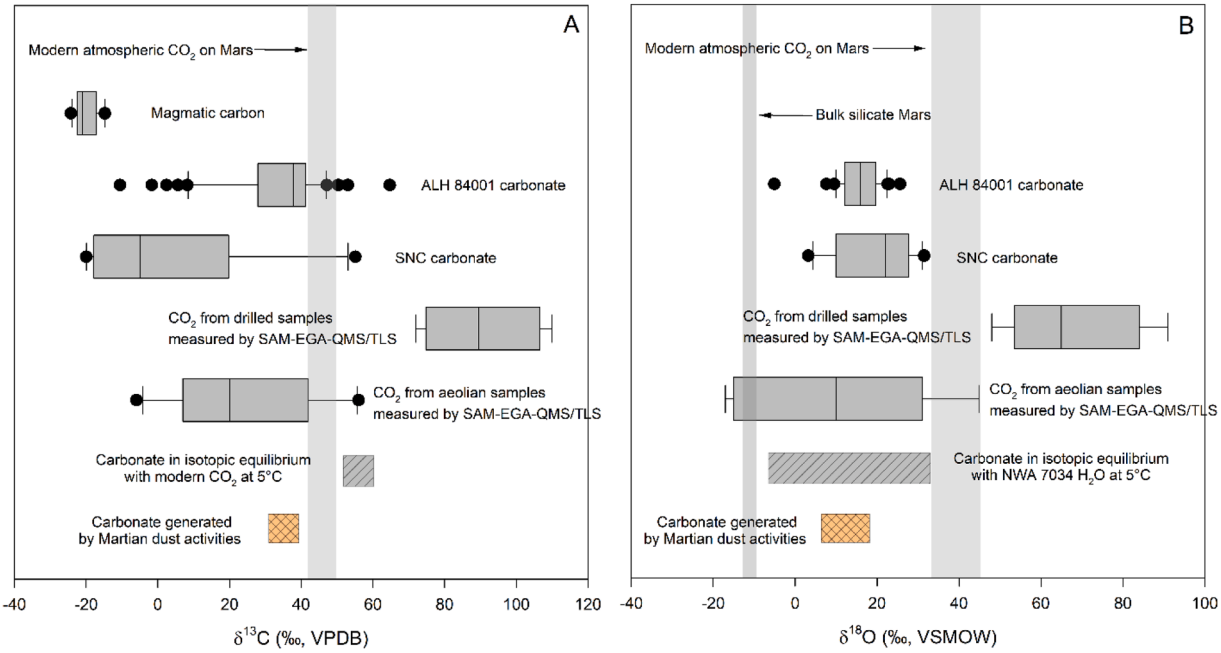

Fig. 4. Comparison of carbon and oxygen isotope compositions in carbonates from the ESD experiments with in-situ and meteorite data from Mars. The carbon (A) and oxygen (B) isotope compositions of carbonate (orange textured bars) generated by Martian dust activities estimated with the isotope composition of modern atmospheric CO_2 on Mars (Webster et al., 2013) and the isotope fractionation factors calibrated in this study. The δ^{13}C and δ^{18}O values of different reservoirs on Mars are also shown for comparison. These reservoirs include CO_2 in the Martian atmosphere (Webster et al., 2013), magmatic carbon (Grady et al., 2004), bulk silicate Mars (Valley et al., 1997), ALH 84,001 carbonate (Romanek et al., 1994; Jull et al., 1995, 1997; Valley et al., 1997; Niles et al., 2005; Shaheen et al., 2015), SNC carbonate (Carr et al., 1985; Jull et al., 1995, 1997; Sharp et al., 2016), CO_2 released from Martian drilled samples measured by SAM-EGA-TLS (Burtt et al., 2024), and CO_2 released from Martian aeolian samples measured by SAM-EGA-QMS/TLS (Leshin et al., 2013; Franz et al., 2020). Gray textured bars in (a) represent the range of carbonate with the isotope compositions in equilibrium with modern atmospheric CO_2 at 5 °C, and those in (B) represent the water evolved from SNC meteorite NWA 7034 during stepped heating experiments (Agee et al., 2013).

evaporative Rayleigh fractionation and cryogenic precipitation (Burtt et al., 2024).

Our experimental results indicate that carbonate minerals on Mars' surface may be formed by ESD-driven processes involving CO_2 radicals (CO^*, CO_2^+) and excited O_I^* (^{1}D, ^{3}P, and ^{5}P) based on in situ plasma spectroscopy. The CO_2-carbonate carbon and oxygen isotope

fractionations measured in our ESD experiments ($\varepsilon^{13}C = -11.4$ ‰, $\varepsilon^{18}O = -22.8$ ‰) are all negative, indicating that substantial kinetic isotope effects occur during the ESD-driven formation of carbonate minerals. The magnitude of these isotope effects, given the measured isotopic composition of CO_2 in the Martian atmosphere, could produce carbonate minerals having $\delta^{13}C$ and $\delta^{18}O$ values within the range reported for carbonate minerals in Mars meteorites, especially the aeolian samples (Fig. 4). The carbonates generated by ESD processes are depleted in ^{13}C, which should be taken into account when using the $\delta^{13}C$ of Martian atmospheric CO_2 as a constraint for carbon fluxes among various sinks, such as escape to space or incorporation in carbonates or organic matter (Hu et al., 2015; Alday et al., 2023; Ueno et al., 2024).

Due to the lack of high-precision $\Delta^{17}O$ data for Martian atmospheric CO_2, it remains unclear whether the $\Delta^{17}O$ anomaly observed in carbonate minerals from Martian meteorites is inherited from atmospheric CO_2 with an anomalous $\Delta^{17}O$ signature or results from non-mass-dependent isotope effects during carbonate formation. Although O_3 was detected in ESD-in-CO_2 (Wu et al., 2018), its quantity relative to O_I* (from CO_2) may not be large enough to affect the $\Delta^{17}O$ value of ESD-generated $MgCO_3$ (Table 3).

Overall, we found that the products of ESD-induced heterogeneous electrochemical processes, analogous to those potentially associated with Martian dust activities, all show some extent of depletion in the heavy isotopes ^{37}Cl, ^{18}O, and ^{13}C. This phenomenon indicates the ubiquitous occurrence of mass-dependent kinetic isotope fractionation involved in the generation of volatile species (Cl_I*, O_I*, CO_2^+, and CO*) through the breakdown of chlorides and CO_2 upon impact by energetic electrons. Apparently, the energetic electrons from ESD impact chloride mineral grains and collide with CO_2 molecules in the atmosphere, which causes the release of volatiles (Cl_I*) and free radicals (O_I*, CO*, CO_2^+, O_3) that are heavy-isotope depleted, and these reactive species become incorporated into secondary mineral products (e.g., chlorides, oxychlorides, and carbonates). The mass-dependent kinetic isotope effects observed in products of ESD-driven experiments under Mars-like conditions are generally of opposite sign to equilibrium isotope effects and to isotope effects observed in products of ozone- and UV-driven reactions in aqueous media. Comparisons of the present ESD experimental results with available isotopic data from Mars atmosphere, surface materials, and meteorites indicate that ESD-driven processes are likely to play a substantial role in atmosphere-surface interactions on Mars.

5. Conclusion

A conceptual model of the global Cl cycle and air-borne carbonates in the contemporary Mars surface-atmosphere system based on the results of the present study (i.e., the transfer of isotopic signatures that are consistent with mission observations) is shown in Fig. 5. Although other chemical reaction processes may be involved in the generation of the isotopically depleted chloride, (per)chlorate, and carbonate minerals observed at Mars' surface, mass-balance calculations (Wang et al., 2023)

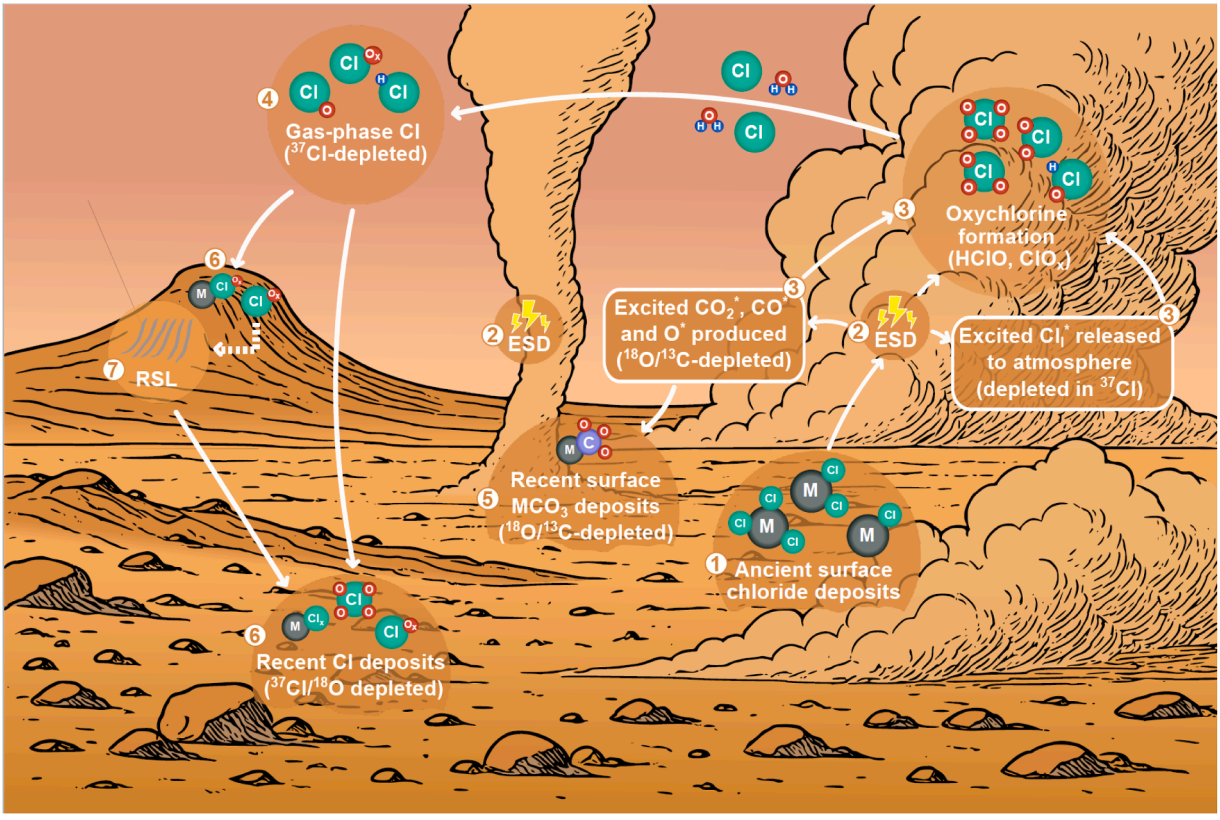

Fig. 5. A conceptual model of the Mars global contemporary surface-atmosphere Cl cycle and air-borne carbonates that is consistent with the results of the present study (i.e., the transfer of isotopic signatures). (1 & 2) The HEC induced by dust-driven ESD partially decomposes the surface chloride mineral; (3) HEC produces volatile Cl_I* (^{37}Cl-depleted) from chlorides; along with ^{13}C- and ^{18}O-depleted species CO_2^+ CO* and O* from CO_2; and minor amounts of (per)chlorate, carbonate, and activated oxide are also formed by HEC reactions but with lower conversion rates than the volatile species; (4) the atmospheric HEC products (with depleted ^{37}Cl, consistent with mission observations (Liuzzi et al., 2021; Trokhimovskiy et al., 2021)) are deposited onto the surface, forming new (per)chlorate, chloride, and carbonate mineral deposits (Wu et al., 2018; Wang et al., 2023) having isotopic depletions in ^{37}Cl, ^{18}O, and ^{13}C, consistent with mission observations (Farley et al., 2016; Leshin et al., 2013; Franz et al., 2020). In addition, there is a possibility that the Cl-bearing products deposited on the Martian surface could lead to the formation of Cl-salt rich brines that may percolate below the subsurface and flow out in the form of (7) RSL (recurring slope lineae) that generated the modern Cl-deposits (6) (Wang et al., 2019). As chloride salt rich deposits are modified by ongoing dust-driven HEC, the progressive depletion of ^{37}Cl would continue, leading further towards the negative δ^{37}Cl values observed in surface Cl-bearing minerals by SAM-Curiosity on Mars (Farley et al., 2016).

show that the inventories of these secondary minerals can be accounted for entirely by ESD processes associated with dust activities on Mars. The comparison of isotopic results of the present study and those of in situ measurements on Mars and of Martian meteorites supports the hypothesis that heterogeneous electrochemistry induced by dust-driven ESD is responsible for the formation of secondary chlorides, (per)chlorates, and carbonates at the surface of Mars. Further isotopic investigations of Martian surface materials by lander missions and sample returns are needed to better understand the global cycles of chlorine, carbon, and oxygen on Mars. Given the ubiquity of dust activity and the known low-breakdown electric field threshold (Melnik and Parrot, 1998; Rahman et al., 2023) on Mars, dust-induced electrochemistry may represent a dominant, yet underappreciated, force driving chemical evolution in the modern Martian near-surface environment.

The results of this study also offer new insight into the origin of Martian carbonates, suggesting that not all of them formed under ancient, water-rich conditions. While many carbonates in meteorites and sedimentary rocks have been attributed to water-rich surface conditions that existed early in Martian history, our results show that ESD-driven reactions can also generate carbonates under the modern hyperarid conditions. The experimentally observed kinetic isotope effects produce $\delta^{13}C$ and $\delta^{18}O$ values consistent with those in near-surface carbonates, particularly in aeolian materials in mission observations (Leshin et al., 2013). Distinguishing carbonates formed in aqueous environments from those formed by ESD-driven reactions under dry conditions may be possible through detailed examination of depositional settings, mineralogy, and textural features of intact rock and sediment cores from the surface of Mars.

Credit: author contribution statement

AW and YCY conducted ESD experiments in the simulation chamber and collected the plasma spectra. HKQ, AW made the plasma line assignment. AWJ purified the oxychlorines products. NCS, LJH did the Cl and O isotope analyses of the ESD-produced oxychlorines. HY, YW purified and did the C and O isotope analyses of the ESD-produced carbonates, under the supervision of HMB. KSO contributed to bringing the TGO isotope data into this study and generated Fig. 5 with the input from all coauthors. NCS, HY, and AW drafted the manuscript with the input and suggestions from all coauthors.

Data and materials availability

All data needed to evaluate the conclusions in the manuscript are present in the manuscript and the Supplementary Materials. In addition, the digital data of plasma spectra in situ collected during ESD process, as well as the measured ESD parameters (V ~ I) are saved in several Excel files, which are available at a permanent repository website curated by the Olin library of Washington University in St. Louis at https://doi.org/10.7936/6rxs-108284.

Funding

The scientific investigation reported in the manuscript are mainly supported by NASA Solar System Working (SSW) program SSW-80NSSC17K-0776 and 80NSSC21K-1832 project (to AW). This study is also benefited from the NASA support for the science Co-I of the ESA-led ExoMars Rosalind Franklin Mission (JPL subcontract #1295053). HY, HB and YW's research was supported by NSFC grants W2441015, 42494851 and Fundamental Research Funds for the Central Universities (0206/14380232). KSO acknowledges funding from the UK Space Agency (ST/T002069/1, ST/Y000196/1).

CRediT authorship contribution statement

Neil C. Sturchio: Writing – review & editing, Writing – original draft, Visualization, Supervision, Investigation, Conceptualization. **Hao Yan:** Writing – review & editing, Writing – original draft, Visualization, Supervision, Investigation, Conceptualization. **Alian Wang:** Writing – review & editing, Writing – original draft, Visualization, Supervision, Investigation, Conceptualization. **W. Andrew Jackson:** Writing – review & editing, Investigation, Conceptualization. **Huiming Bao:** Writing – review & editing, Supervision, Investigation, Conceptualization. **Chuck Y.C. Yan:** Writing – review & editing, Methodology. **Linnea J. Heraty:** Writing – review & editing, Methodology. **Yu Wei:** Writing – review & editing, Methodology. **Quincy H.K. Qu:** Writing – review & editing, Visualization. **Kevin S. Olsen:** Writing – review & editing, Visualization.

Declaration of competing interest

The authors declare the following financial interests/personal relationships which may be considered as potential competing interests:

Dr. Huiming Bao, co-author of this manuscript, is a Co-Chief Editor of Earth and Planetary Science Letters. Given his role, Dr. Bao had no involvement in the peer review of this article and had no access to information regarding its peer review. Full responsibility for the editorial process for this article was delegated to another journal editor. If there are other authors, they declare that they have no known competing financial interests or personal relationships that could have appeared to influence the work reported in this paper.

Acknowledgements

Mhairi Reid, University of Oxford, is thanked for help in preparing Fig. 5. Two anonymous reviewers provided insighful comments that led to an improved manuscript.

Supplementary materials

Supplementary material associated with this article can be found, in the online version, at doi:10.1016/j.epsl.2025.119784.

Data availability

Data are available at an online repository.

References

Agee, C.B., Wilson, N.V., McCubbin, F.M., Ziegler, K., Polyak, V.J., Sharp, Z.D., ASmerom, Y., Nunn, M.H., Shaheen, R., Thiemens, M.H.>., Steele, A., Fogel, M.L., Bowden, R., Glamclija, M.A., Zhang, Z., Elardo, S.M., 2013. Unique meteorite from early amazonian Mars: water-rich basaltic breccia Northwest Africa 7034. Science 339, 780–785. https://doi.org/10.1126/science1228858.

Alday, J., Trokhimovskiy, A., Patel, M.R., Federova, A.A., Lefevre, F., MOntmessin, F., Holmes, J.A., Ralendran, K., Mason, J.P., Olsen, K.S., Belyaev, D.A., Korablev, O., Baggio, L., Patrakeev, A., Shakun, A., 2023. Photochemical depletion of heavy CO isotopes in the Martian atmosphere. Nat. Astronom. 7, 867–876. https://doi.org/10.1038/s41550-023-01974-2.

Bak, E.N., Nørnberg, P., SJensen, S.J.K., Thøgersen, J., Finster, K., 2022. Physical and chemical mechanisms that impact the detection, identification, and quantification of organic matter and the survival of microorganisms on the Martian surface–a review. Intl. J. Astrobiol. 21, 356–379. https://doi.org/10.1017/S1473550421000392.

Beck, W.C., Grossman, E.L., Morse, J.W., 2005. Experimental studies of oxygen isotope fractionation in the carbonic acid system at 15, 25, and 40 °C. Geochim. Cosmochim. Acta 69, 3493–3503. https://doi.org/10.1016/j.gca.2005.02.003.

Bellucci, J.J., Whitehouse, M.J., John, T., Nemchin, A.A., SNope, J.F., Bland, P.A., Benedix, G.K., 2017. Halogen and Cl isotopic systematics in Martian phosphates: implications for the Cl cycle and surface halogen reservoirs on Mars. Earth Planet. Sci. Lett. 458, 192–202. https://doi.org/10.1016/j.epsl.2016.10.028.

Böhlke, J.K., Mroczkowski, S.J., Sturchio, N.C., Heraty, L.J., Richman, K.W., Sullivan, D. B., Griffith, K.N., Gu, B., Hatzinger, P.B., 2017. Stable isotope analyses of oxygen (^{18}O: ^{17}O: ^{16}O) and chlorine (^{37}Cl: ^{35}Cl) in perchlorate: reference materials, calibrations, methods, and interferences. Rapid Comm. Mass Spec. 31, 85–110. https://doi.org/10.1002/rcm7751.

Burtt, D.G., Stern, J.C., WEbster, C.R., Hofmann, A.E., Franz, H.B., Sutter, B., Thorpe, M. T., Kite, E.S., Eigenbrode, J.L., Pavlov, A.A., House, C.H., Tutolo, B.M., Des Marais, D.J., RAmpe, E.B., McAdam, A.C., Malespin, C.A., 2024. Highly enriched

carbon and oxygen isotopes in carbonate-derived CO_2 at Gale crater, Mars. Proc. Natl. Acad. Sci. 121, e2321342121. https://doi.org/10.1073/pnas.2321342121.
Carr, R., Grady, M., Wright, I., Pillinger, C., 1985. Martian atmospheric carbon dioxide and weathering products in SNC meteorites. Nature 314, 248–250.
Chacko, T., Cole, D.R., Horita, J., 2001. Equilibrium oxygen, hydrogen and carbon isotope fractionation factors applicable to geologic systems. Rev. Mineral. Geochem. 43, 1–81. https://doi.org/10.2318/gsrmg.43.1.1.
Clark, I.D., Fontes, J.-C., Fritz, P., 1992. Stable isotope disequilibria in travertine from high pH waters: laboratory investigations and field observations from Oman. Geochim. Cosmochim. Acta 56, 2041–2050.
Clark, I.D., Lauriol, B., 1992. Kinetic enrichment of stable isotopes in cryogenic calcites. Chem. Geol. 102, 217–228.
Eden, H.F., Vonnegut, B., 1973. Electrical breakdown caused by dust motion in low-pressure atmospheres: considerations for Mars. Science 180, 962–963.
Ehlmann, B., Mustard, J., Murchie, S.L., 2010. Geologic setting of serpentine deposits on Mars. Geophys. Res. Lett. 37, L06201. https://doi.org/10.1029/2010GL042596.
Endoh, M., Tsuji, M., Nishimura, Y., 1982. CO_2^+ ((A-X and B-X) emissions resulting from the He (2^3S) + CO_2 penning ionization. J. Chem. Phys. 77, 4027–4031.
Estrada, N.L., Anderson, T.A., Böhlke, J.K., Gu, B., Hatzinger, P.B., Mroczkowski, S.J., Rao, B., Sturchio, N.C., Jackson, W.A., 2021. Origin of the isotopic composition of natural perchlorate: experimental results for the impact of reaction pathway and initial ClOx reactant. Geochim. Cosmochim. Acta 311, 292–315. https://doi.org/10.1016/j.gca.2021.06.039.
Farley, K.A., Martin, P., ARcher Jr., P.D., Atreya, S.K., COnrad, P.G., Eigenbrode, J.L., Fairen, A.G., Franz, H.B., Freissinet, C., Glavin, D.P., Mahaffy, P.R., Malespin, C., Ming, D.W., Navarro-Gonzalez, R., Sutter, B., MSL Science Team, 2016. Light and variable $^{37}Cl/^{35}Cl$ ratios in rocks from Gale Crater, Mars: possible signature of perchlorate. Earth Planet Sci Lett. 438, 14–24. https://doi.org/10.1016/j.epsl.2015.12.013.
Farquhar, J., Thiemens, M.H., 2000. Oxygen cycle of the Martian atmosphere-regolith system: $\Delta^{17}O$ of secondary phases in Nakhla and Lafayette. J. Geophysi. Res.: Planets 105, 11991–11997.
Franz, H.B., Mahaffy, P.R., WEbster, C.R., Flesch, G.J., Raaen, E., Freissinet, C., Atreya, S. K., House, C.H., McAdam, A.C., Knudson, C.A., ARcher Jr., P.D., Stern, J.C., Steele, A., Sutter, B., Eigenbrode, J.L., Glavin, D.P., Lewis, J.M.T., Malespin, C.A., Millan, M., Ming, D.W., Navarro-Gonzalez, R., Summons, R.E., 2020. Indigenous and exogenous organics and surface–atmosphere cycling inferred from carbon and oxygen isotopes at Gale crater. Nat. Astron. 4, 526–532. https://doi.org/10.1038/s41550-019-0990-x.
Glavin, D.P., Freissinet, C., Miller, K.E., Eigenbrode, J.L., Brunner, A.E., Buch, A., Sutter, B., Archer Jr., P.D., Atreya, S.K., Brinckerhoff, W.B., Cabane, M., Coll, P., COnrad, P.G., COscia, D., Dworkin, J.P., Franz, H.B., Grotzinger, J.P., Leshin, L.A., Martin, M.G., McKay, C., Ming, D.W., Navarro-Gonzalez, R., PAvlov, A., Steele, A., Summons, R.E., Szopa, C., Teinturier, S., Mahaffy, P.R., MSL Science Team, 2013. Evidence for perchlorates and the origin of chlorinated hydrocarbons detected by SAM at the Rocknest aeolian deposit in Gale Crater. J. Geophys. Res.: Planets 118, 1955–1973. https://doi.org/10.1002/jgre.20144.
Grady, M., Verchovsky, A., Wright, I., 2004. Magmatic carbon in Martian meteorites: attempts to constrain the carbon cycle on Mars. Intl. J. Astrobiol. 3, 117–124. https://doi.org/10.1017/S1473550404002071.
Gu, B., Böhlke, J.K., Sturchio, N.C., Hatzinger, P.B., Jackson, W.A.>., Beloso Jr., A.D., Heraty, L.J., Bian, Y., Jiang, X., Brown, G.M., 2011. Applications of selective ion exchange for of perchlorate removal, recovery, and environmental forensics. In: Sengupta, A.K. (Ed.), Ion Exchange and Solvent Extraction: A Series of Advances, Ion Exchange and Solvent Extraction: A Series of Advances, 21. CRC Press, pp. 117–144.
Hatzinger, P.B., Böhlke, J.K., Sturchio, N.C., Izbicki, J., Teague, N., 2018. Four-dimensional isotopic approach to identify perchlorate sources in groundwater: application to the Rialto-Colton and Chino subbasins, southern California (USA). Appl. Geochem. 97, 213–225. https://doi.org/10.1016/j.apgeochem.2018.08.020.
Hilkert, A., Böhlke, J.K., Mroczkowski, S.J., Fort, K.L., Aizikov, K., Wang, X.T., Kopf, S. H., Neubauer, C., 2021. Exploring the potential of electrospray-orbitrap for stable isotope analysis using nitrate as a model. Anal. Chem. 93, 9139–9148. https://doi.org/10.1021/acs.analchem.1c00944.
Hokazono, H., Obara, M., Midorikawa, K., Tashiro, H., 1991. Theoretical operational life study of the closed-cycle transversely excited atmospheric CO_2 laser. J. Appl. Phys. 69, 6850–6868.
Hu, R., Kass, D.M., Ehlmann, B.L., Yung, Y.L., 2015. Tracing the fate of carbon and the atmospheric evolution of Mars. Nat. Commun. 6, 10003. https://doi.org/10.1038/ncomms10003.
Jackson, T.L., Farrell, W.M., Delory, G.T., Nithianandam, J., 2010. Martian dust devil electron avalanche process and associated electrochemistry. J. Geophys. Res.: Planets 115, E05006. https://doi.org/10.1029/2009JE003396.
Jackson, W.A., Brundrett, M., Böhlke, J.K., Hatzinger, P.B., Mroczkowski, S.J., Sturchio, N.C., 2021. Isotopic composition of natural and synthetic chlorate ($\delta^{18}O$, $\Delta^{17}O$, $\delta^{37}Cl$, $^{36}Cl/Cl$): methods and initial results. Chemosphere 274, 129586. https://doi.org/10.1016/j.chemosphere.2021.129586.
Jull, A., Eastoe, C., Cloudt, S., 1997. Isotopic composition of carbonates in the SNC meteorites, Allan Hills 84001 and Zagami. J. Geophys. Re.: Planets 102, 1663–1669.
Jull, A., Eastoe, C., Xue, S., Herzog, G., 1995. Isotopic composition of carbonates in the SNC meteorites Allan Hills 84001 and Nakhla. Meteoritics 30, 311–318.
Kramida, A., Ralchenko, Y., Reader, J., NIST ASD Team, 2024. NIST Atomic Spectra Database (ver. 5.11). [Online]. National Institute of Standards and Technology, Gaithersburg, MD. https://doi.org/10.18434/T4W30F. Available. https://physics.nist.gov/asd [20 January 2023].
Leshin, L.A., Mahaffy, P.R., WEbster, C.R., Cabane, M., Coll, P., Conrad, P.G., ARcher Jr., P.D., Atreya, S.K., Brunner, A.E., Buch, A., Eigenbrode, J.L., FLesch, G.J., Franz, H.B., Freissinet, C., Glavin, D.P., McAdam, A.C., Miller, K.E., Ming, D.W., Morris, R.V., Navarro-Gonzalez, R., Niles, P.B., Owen, T., Pepin, R.O., Squyres, S., Steele, A., Stern, J.C., Summons, R.E., Sumner, D.Y., Sutter, B., Szopa, C., Teinturier, S., Trainer, M.G., Wray, J.J., Grotzinger, J.P., MSL Science Team, 2013. Volatile, isotope, and organic analysis of martian fines with the Mars Curiosity rover. Science 341, 1238937. https://doi.org/10.1126/science.1238937.
Liuzzi, G., Villanueva, G.L., Viscardy, S., Mege, D., Crismani, M.M.J., Aoki, S., Gurgurewicz, J., Tesson, P.-A., Mumma, M.J., Smith, M.D.>., Faggi, S., Kofman, V., Knutsen, E.W., Daerden, F., Neary, L., SChmidt, F., Trompet, L., ERwin, J.T., Robert, S., Thomas, I.R., Ristic, B., Belucci, G., Lopez-Moreno, J.J., Patel, M.R., Vanaele, A.C., 2021. Probing the atmospheric Cl isotopic ratio on Mars: implications for planetary evolution and atmospheric chemistry. Geophys. Research Lett. 48, e2021GL092650. https://doi.org/10.1029/2021GL092650.
Lofthus, A., Krupenie, P.H., 1977. The spectrum of molecular nitrogen. J.Phys. Chem. Ref. Data 6, 113–307.
Lukes, P., Cllupek, M., Babicky, V., Simek, M., Tothova, I., Janda, V., Moucha, T., Kordac, M., 2008. Role of solution conductivity in the electron impact dissociation of H2O induced by plasma processes in the pulsed corona discharge in water. In: HAKONE XI, 11th International Symposium on High Pressure, Low Temperature Plasma Chemistry, Contributed Papers, Oleron Island.
Marlier, J.F., O'Leary, M.H., 1984. Carbon kinetic isotope effects on the hydration of carbon dioxide and the dehydration of bicarbonate ion. J. Amer. Chem. Soc. 106, 5054–5057.
McCrea, J.M., 1950. On the isotopic chemistry of carbonates and a paleotemperature scale. J. Chem. Phys. 18, 849–857.
Melnik, O., Parrot, M., 1998. Electrostatic discharge in Martian dust storms. J. Geophys. Res.: Space Phys. 103, 29107–29117.
Mills, A., 1977. Dust clouds and frictional generation of glow discharges on Mars. Nature 268, 614. -614.
Mook, W., Bommerson, J., Staverman, W., 1974. Carbon isotope fractionation between dissolved bicarbonate and gaseous carbon dioxide. Earth Planet. Sci. Lett. 22, 169–176.
Niles, P., Leshin, L., Guan, Y., 2005. Microscale carbon isotope variability in ALH84001 carbonates and a discussion of possible formation environments. Geochim. Cosmochim. Acta. 69, 2931–2944. https://doi.org/10.1016/j.gca.2004.12.012.
Pearse, R.W.B., Gaydon, 1976. The Identification of Molecular Spectra. Fourth Edition. Chapman and Hall, London, p. 407.
Rahman, M.M., Saieed, A., Hickey, J.-P., 2023. Turbulence-induced electrical discharges in charged particle-laden Martian boundary layers. Flow 3, E34. https://doi.org/10.1017/flo.2023.28.
Romanek, C., Grady, M.M., Wright, I.P., Mittlefehldt, D.W., Socki, R.A., Pillinger, C.T., Gibson Jr., E.K., 1994. Record of fluid–rock interactions on Mars from the meteorite ALH84001. Nature 372, 655–657.
Romanek, C.S., Grossman, E.L., Morse, J.W., 1992. Carbon isotopic fractionation in synthetic aragonite and calcite: effects of temperature and precipitation rate. Geochim. Cosmochim. Acta 56, 419–430.
Shaheen, R., Abramian, A., Horn, J., Dominguez, G., Sullivan, R., Thiemens, M.H., 2010. Detection of oxygen isotopic anomaly in terrestrial atmospheric carbonates and its implications to Mars. Proc. Natil. Acad. Sci. 107, 20213–20218. https://doi.org/10.1073/pnas.1014399107.
Shaheen, R., Niles, P.B., Chong, K., Corrigan, C.M., Thiemens, M.H., 2015. Carbonate formation events in ALH 84001 trace the evolution of the Martian atmosphere. Proc. Natl. Acad. Sci 112, 336–341. https://doi.org/10.1073/pnas.1315615112.
Sharp, Z., Williams, J., Shearer, C., Agee, C., McKeegan, K., 2016. The chlorine isotope composition of Martian meteorites 2. Implications for the early solar system and the formation of Mars. Meteoritics Planet. Sci. 51, 2111–2126. https://doi.org/10.1111/maps.12591.
Skalny, J., Matejcik, S., Orszagh, J., Vladoiu, R., Mason, N., 2007. A study of the physical and chemical processes active in ozone generation by carbon dioxide fed corona discharges. Ozone: Science and Engineering 29, 399–404. https://doi.org/10.1080/01919510701577237.
Steele, A., McCubbin, F.M., Fries, M., Kater, L., Boctor, N.Z., Fogel, M.L., Conrad, P.G., Glamoclija, M., Spencer, M., Morrow, A.L., Hammond, M.R., Zare, R.N., Vicenzi, E. P., Siljeström, S., Bowden, R., Herd, C.D.K., Mysen, B.O., Shirey, S.B., Amundsen, H. E.F., Treiman, A.H., Bullock, E.S., Jull, A.J.T., 2012. A reduced organic carbon component in Martian basalts. Science 337, 212–215. https://doi.org/10.1126/science.1220715.
Sturchio, N.C., Böhlke, J.K., Gu, B., Horita, J., Brown, G.M., Beloso Jr., A.D., Patterson, L. J., Hatzinger, P.B., Jackson, W.A., Batista, J., 2006. Stable isotopic composition of chlorine and oxygen in synthetic and natural perchlorate. Ch. 5. In: Gu, B., Coates, J. D. (Eds.), Perchlorate: Environmental Occurrence, Interactions and Treatment. Springer, New York, pp. 93–109.
Trokhimovskiy, A., Federova, A.A., Olsen, K.S., Alday, J., Korablev, O., Montmessin, F., Lefevre, F., Patrakeev, A., Belyaev, D., Shakun, A.V., 2021. Isotopes of chlorine from HCl in the Martian atmosphere. Astron. Astrophys. 651, A32. https://doi.org/10.1051/0004-6361/202140916.
Ueno, Y., Schmidt, J.A., Johnson, M.S., Zang, X., Gilbert, A., Kurokawa, H., Usui, T., Aoki, S., 2024. Synthesis of 13C-depleted organic matter from CO in a reducing early Martian atmosphere. Nat. Geosci. 17, 503–507. https://doi.org/10.1038/s41561-024-01443-z.
Valley, J.W., Eiler, J.M., Graha, C.M., Gibson, E.K., Romanek, C.S., Stolper, E.M., 1997. Low-temperature carbonate concretions in the martian meteorite ALH84001: evidence from stable isotopes and mineralogy. Science 275, 1633–1638.
Wang, A., Jackson, W.A., Sturchio, N.C., Houghton, J., Yan, C.Y.C., Olsen, K.S., Qu, Q.H. K., 2023. Quantification of carbonates, oxychlorines, and chlorine generated by

heterogeneous electrochemistry induced by martian dust activity. Geophys. Res. Lett. 50, e2022GL102127. https://doi.org/10.1029/2022GL102127.

Wang, A., Ling, Z., Yan, Y., McEwen, A.S., Mellon, M.T., Smith, M.D., Jolliff, B.L., Head, J., 2019. Subsurface Cl-bearing salts as potential contributors to recurring slope lineae (RSL) on Mars. Icarus 333, 464–480. https://doi.org/10.1016/j.icarus.2019.06.024.

Wang, A., Yan, Y., Dyar, D.M., Houghton, J.L., Farrell, W.M., Jolliff, B.L., McLennan, S. M., Shi, E., Qu, H., 2020. Amorphization of S, Cl-salts induced by Martian dust activities. J. Geophys. Res.: Planets 125, e2020JE006701. https://doi.org/10.1029/2020JE006701.

Webster, C.R., Mahaffy, P.R., Flesch, G.J., Niles, P.B., Jones, J.H., Leshin, L.A., Atreya, S. K., Stern, J.C., Christensen, L.E., Owen, T., Franz, H., Pepin, R.O., Steele, A., 2013. Isotope ratios of H, C, and O in CO_2 and H_2O of the Martian atmosphere. Science 341, 260–263.

Wei, Y., Yan, H., Peng, Y., Bao, H., 2024a. Quantitative conversion of sulfate oxygen for high-precision triple oxygen isotope analysis. Anal. Chem. 96, 19387–19395. https://doi.org/10.1021/acs.analchem.4c03683.

Wei, Y., Yan, H., Peng, Y., Han, S., Bao, H., 2024b. Thermal-gradient-induced isotope fractionation during CO_2-O_2 triple oxygen isotope exchange. Geochim. Cosmochim. Acta 370, 29–40. https://doi.org/10.1016/j.gca.2024.02.010.

Williams, J.T., Shearer, C.K., Sharp, Z.D., Burger, P.V., McCubbin, F.M., SAntos, A.R., Agee, C.B., McKeegan, K.D., 2016. The chlorine isotopic composition of Martian meteorites 1: chlorine isotope composition of Martian mantle and crustal reservoirs and their interactions. Meteoritics Planet. Sci. 51, 2092–2110. https://doi.org/10.1111/maps.12647.

Wu, Z., Wang, A., Farrell, W.M., Yan, Y., Wang, K., Houghton, J., Jackson, W.A., 2018. Forming perchlorates on Mars through plasma chemistry during dust events. Earth Planet. Sci. Lett. 504, 94–105. https://doi.org/10.1016/j.epsl.2018.08.040.

Yan, H., Liu, Z., Sun, H., 2020. Large degrees of carbon isotope disequilibrium during precipitation-associated degassing of CO_2 in a mountain stream. Geochim. Cosmochim. Acta 273, 244–256. https://doi.org/10.1016/j.gca.2020.01.012.